Published in final edited form as:
J Biomech. 2009 August 25; 42(12): 1909–1916. doi:10.1016/j.jbiomech.2009.05.018.

Stress-Strain Behavior of Mitral Valve Leaflets in the Beating Ovine Heart

Gaurav Krishnamurthy[*,§], **Akinobu Itoh**[*], **Wolfgang Bothe**[*], **Julia C. Swanson**[*], **Ellen Kuhl**[§], **Matts Karlsson**[†], **D. Craig Miller**[*], and **Neil B. Ingels Jr.**[#,*]

[*]Department of Cardiothoracic Surgery, Stanford University School of Medicine, Stanford, CA

[§]Department of Mechanical Engineering, Stanford University, Stanford, CA

[†]Department of Management and Engineering, Linköping University, Linköping, Sweden

[#]Laboratory of Cardiovascular Physiology and Biophysics, Research Institute of the Palo Alto Medical Foundation, Palo Alto, CA

Abstract

Excised anterior mitral leaflets exhibit anisotropic, nonlinear material behavior with pre-transitional stiffness ranging from 0.06-0.09 N/mm^2 and post-transitional stiffness from 2-9 N/mm^2. We used inverse finite element (FE) analysis to test, for the first time, whether the anterior mitral leaflet (AML), *in vivo*, exhibits similar non-linear behavior during isovolumic relaxation (IVR). Miniature radiopaque markers were sewn to the mitral annulus, AML, and papillary muscles in 8 sheep. 4-D marker coordinates were obtained using biplane videofluoroscopic imaging during three consecutive cardiac cycles. A FE model of the AML was developed using marker coordinates at the end of isovolumic relaxation (when pressure difference across the valve is approximately zero), as the reference state. AML displacements were simulated during IVR using measured left ventricular and atrial pressures. AML elastic moduli in the radial and circumferential directions were obtained for each heartbeat by inverse FEA, minimizing the difference between simulated and measured displacements. Stress-strain curves for each beat were obtained from the FE model at incrementally-increasing transmitral pressure intervals during IVR. Linear regression of 24 individual stress-strain curves (8 hearts, 3 beats each) yielded a mean (±SD) linear correlation coefficient (r^2) of 0.994±0.003 for the circumferential direction and 0.995±0.003 for the radial direction. Thus, unlike isolated leaflets, the AML, *in vivo*, operates linearly over a physiologic range of pressures in the closed mitral valve.

Keywords

mitral valve; finite element analysis; material properties; anisotropy; elastic modulus

---

Address for Correspondence: Neil B. Ingels, Jr, PhD, Laboratory of Cardiovascular Physiology and Biophysics, Research Institute, Palo Alto Medical Foundation (AMES Building), 795 El Camino Real, Palo Alto, CA 94301-2302, 650.853.4834 FAX 650.324.2665, E-mail: ingels@stanford.edu.

Conflicts of Interest None of the authors have any conflicts of interest.

Introduction

The mitral valve has a dual role during left ventricular (LV) systole in the beating heart. The mitral leaflets, the key components of the valve, must maintain appropriate relative positions and geometry during systole to: (1) seal tightly to prevent regurgitant backflow from the LV into the left atrium; and (2) provide an appropriately-shaped portion of the LV outflow tract. The material properties of the leaflets are of critical importance to both of these tasks, as the varying demands on the heart are met with a wide range of LV pressures and volumes.

The material properties of excised mitral leaflets have been well-characterized (Kunzelman and Cochran, 1992; May-Newman and Yin, 1995; May-Newman and Yin, 1998; Chen, McCulloch et al., 2004; Chen, Yin et al., 2004; He, Sacks et al, 2003; Sacks, He et al, 2002; Sacks, Enomoto et al., 2006; He and Ritchie et al, 2005). In uniaxial studies of excised leaflets, Kunzelman and Cochran (1992) measured highly non-linear stress-strain behavior with distinct pre- and post-transitional regions. In biaxial studies of excised anterior leaflets, May-Newman and Yin (1995) found anisotropic, non-linear material properties with pre-transitional stiffness values ranging from 0.06-0.09 N/mm^2 and post-transitional stiffness values from 2-9 N/mm^2. Recent mitral valve models (Kunzelman, Einstein et al., 2007; Prot, Skallerud et al., 2007; Votta, Caiani et al., 2008) have incorporated these leaflet data into hyperelastic finite element analyses (FEA). Sacks and He (2002) used a left heart simulator and graphite markers to study the *in-vitro* surface strains in the porcine anterior mitral valve leaflets and showed a non-linear relationship between transmitral pressures and leaflet areal strains. The first attempt at quantifying *in-vivo* leaflet strains by Sacks and Enomoto (2006) using a sonmicrometry transducer array showed the same non-linear relationship between pressure and leaflet strains in ovine anterior mitral valve leaflets. Sacks and Enomoto (2006) computed only *in vivo* leaflet strains and did not determine the *in vivo* leaflet elastic moduli or show the relationship between leaflet stresses and leaflet strains for the beating heart.

Recently, we used inverse FEA to obtain the anisotropic elastic moduli of anterior mitral valve leaflets during isovolumic relaxation (IVR) in the beating ovine heart (Krishnamurthy, Ennis et al., 2008). As a first approximation, we assumed a linear relationship between stress and strain during IVR. The present study was undertaken to the test the validity of this assumption.

Methods

All animals received humane care in compliance with the “Principles of Laboratory Animal Care” formulated by the National Society for Medical Research and also in compliance with the “Guide for the Care and Use of Laboratory Animals” prepared by the National Academy of Sciences and published by the National Institutes of Health (U.S. Department of Health and Human Services, NIH Publication 85-23, Revised 1985). This study was approved by the Stanford Medical Center Laboratory Research Animal Preview Committee, which is accredited by the Association for Assessment and Accreditation of Laboratory Animal Care International, and conducted according to Stanford University policy.

Surgical Preparation

Eight adult, Dorsett-hybrid, male sheep (56±8kg) were premedicated with ketamine (25 mg/kg intramuscularly) for venous and arterial catheter placement and monitoring. Anesthesia was induced and maintained with inhalational isoflurane (1-2.5%) and supplemental oxygen. Through a left thoracotomy, 13 miniature tantalum radiopaque markers were implanted in the left ventricle (LV) subepicardial wall silhouetting the LV chamber (Figure 1A). Via a left atriotomy with cardiopulmonary bypass and antegrade cardioplegic arrest, a total of 35 radiopaque tantalum markers were sewn to the following sites: 16 on the atrial aspect of the anterior mitral leaflet (AML) [7 on the AML edge (#1-7, Figure 1B); 9 on the leaflet belly

(#8-16, Figure 1B], 16 around the mitral annulus (Figure 1A), 1 on the central edge of the middle scallop of the posterior mitral leaflet (PML, Figure 1A), and 2 on the anterolateral and posteromedial papillary muscle tips (APM, PPM, Figure 1A). A micromanometer pressure transducer (PA4.5-X6, Konigsberg instruments, Inc., Pasadena, CA, USA) was placed in the LV chamber through the left atrium (LA) and exteriorized.

Data Acquisition

Immediately after the operation, the animals were transferred to the catheterization laboratory and studied in the right lateral decubitus position with the chest open. Two micromanometer-tipped pressure transducers (model MPC-500; Millar Instruments, Houston, TX, USA) were calibrated and inserted into the LV and ascending aorta via a carotid artery catheter, respectively. A Konigsberg pressure transducer was calibrated against the two Millar pressure transducers while all transducers were in the LV, then pulled back into the LA to record left atrial pressure (LAP). Simultaneous biplane videofluoroscopic images (60 Hz, Philips Medical Systems, Pleasanton, CA, USA), ECG, LV pressure (LVP), aortic pressure and LAP were recorded during a hemodynamically stable interval with the heart in normal sinus rhythm and ventilation transiently arrested at end-expiration. At the completion of each study biplane images of a 3D helical phantom of known dimensions spanning the heart space were recorded. The 2D coordinates of each marker in each projection image were digitized frame-by-frame, using semi-automated image processing and digitization software developed in our laboratory (Niczyporuk and Miller, 1991). Data from the two views were merged using the 3D helical phantom image data and software, described previously, and used to yield the 3D marker coordinates (Daughters, Sanders et al., 1989). The accuracy of the 3D reconstructions from biplane videograms of length measurements was previously shown to be 0.1 ± 0.3 mm (Daughters, Sanders et al., 1989).

Hemodynamics and Cardiac Cycle Timing

Three consecutive beats in sinus rhythm were selected for analysis from each heart. For each beat, end-systole (ES) was defined as the frame containing the minimum second derivative of LVP with respect to time during IVR. Negative dP/dt_{max} was computed as the maximum time derivative of LVP during IVR. The onset of isovolumic relaxation (IVR_1, Figure 2) was defined at ES and the end of isovolumic relaxation (IVR_2, Figure 2) as the frame immediately before mitral valve opening, defined as the earliest increase (above the systolic variation) in the separation between the central anterior and posterior leaflet edge markers.

To study the piecewise stress-strain behavior of the anterior mitral leaflet during IVR, for each beat, five frames were selected to span the IVR pressure range, defining four approximately 15 mmHg LVP increments associated with four successive time-intervals (Δt_1-Δt_4) from IVR_2 to IVR_1 (Figure 2). For the 24 beats analyzed, for time-step Δt_1 the group mean (±SD) transmitral pressure gradient (LVP-LAP) ranged from 0 (IVR_2) to 14±1 mmHg; for time-step Δt_2 from 14±1 to 30±5 mmHg; for time-step Δt_3 from 30±5 to 49±6 mmHg; and for time-step Δt_4 from 49±6 to 63±6 mmHg.

Inverse Finite Element Analysis

The inverse finite element analysis methodology to determine the material properties of the anterior mitral valve leaflet has been described in a previous publication (Krishnamurthy, Ennis et al., 2008), thus will only be outlined here.

Finite Element Model—A finite element model of the anterior MV leaflet was developed for each individual time-step (Δt_1, Δt_2 ,Δt_3, Δt_4) and for each beat using Hypermesh version 8.0 SR 1 (Altair Hyperworks; Troy, Michigan) to construct the geometry and meshing of the leaflet and Optistruct version 8.0 SR 1 (Altair; Troy, Michigan) as the solver. Thus 96 individual finite element models (8 hearts, 3 beats/heart, 4 time-steps/beat) were analyzed for this study.

For each beat, the geometry of the anterior leaflet was initially defined by the leaflet marker positions (Figure 1) at IVR_2 (assumed as the minimum-stress reference state). The x, y, z coordinate values for each of the leaflet and annular marker positions at IVR_2 were entered as points in Hypermesh. Five cubic splines were generated through (see Figure 1B): a) Markers 17-1-2-3-4-5-6-7-23; b) Markers 18-8-9-10-11-12-22; c) Markers 19-13-14-15-21; d) Markers 19-16-21; and e) Markers 19-20-21. These splines were used to generate a bicubic leaflet surface.

For the purpose of defining the MV leaflet material properties for Δt_1, a coordinate system was defined with origin at the center of the 16 markers defining the saddle-shaped annulus (Levine, Handschumacher et al., 1989) at IVR_2. A line from the origin to marker #20 (the "saddlehorn") was defined as the leaflet radial axis (R, Figure 1). The leaflet circumferential axis (C, Figure 1) was defined normal to R and in the plane containing R and the posterior commissural marker (#23, Figure 1).

A homogeneous leaflet was assumed, with an orthotropic linear elastic material model (MAT8 in Hypermesh). The bicubic surface fit of the MV leaflet was then meshed with plane-stress quadrilateral shell elements. A typical anterior leaflet was meshed with 2200 elements yielding an element size of 0.004 cm^2.

The strut chordae were defined as structures undergoing pure tension (MAT1 in Hypermesh). A previously published *ex vivo* modulus (elastic modulus = 20 N/mm^2; cross sectional area = 0.008 cm^2 (Kunzelman and Cochran, 1992)) was used for the strut chordae. Tension-only bar elements (PBARL in Hypermesh) were defined as radiating from the papillary muscle tip marker points (APM & PPM, Figure 1A) to leaflet belly insertion positions (Figure 3) defined from anatomical photographs.

The boundary conditions were then enforced on the finite element model. The measured transmitral pressure gradient (LVP-LAP) for the first time-step (Δt_1) was applied to the anterior mitral leaflet. The displacements of the annular markers (#17-23, Figure 1B), anterior leaflet edge markers (#1-7, Figure 1B) and papillary tip markers (APM & PPM, Figure 1A) were defined using actual marker data at the end of Δt_1.

The Hypermesh finite element model (Figure 3) was then solved for the enforced boundary conditions using Optistruct to obtain the simulated displacements of the leaflet belly markers (#8-16, Figure 1B). This initial run assumed nominal anterior leaflet material properties obtained from previous *ex vivo* studies (Kunzelman and Cochran, 1992).

Inverse Finite Element Analysis Algorithm—The Optistruct solver was then interlinked with commercial optimization software, Hyperstudy version 8.0 SR 1 (Altair Hyperworks, Troy, Michigan) to run an inverse finite element analysis to yield the *in vivo* material properties of the mitral valve during Δt_1. In this algorithm, the model-simulated displacements of the nine leaflet belly markers (#8-16, Figure 1B) from the nominal run were compared with the actual measured displacements of these 9 markers during time-step Δt_1 to yield a response function defined as the root mean squared (RMS) displacement difference between measured and actual displacements of the nine leaflet belly markers. Hyperstudy then used a parameter identification algorithm, the "Method of Feasible Directions" (Belegundu, Damle et al., 2004), to minimize the response function by repeated iterations of the material properties (E_{circ}, E_{rad}) in the finite element model until a global minimum was obtained (Figure 4). Leaflet circumferential-radial shear during IVR proved sufficiently small that E_{circ} and E_{rad} values so obtained were unchanged with inclusion or exclusion of this shear in the parameter identification process. The material property values (E_{circ}, E_{rad}) obtained at the end of the material identification run with the response function at its global minimum were interpreted as the *in vivo* material properties of the anterior MV leaflet belly during Δt_1. That is, these material property values, when used in the finite element model for the anterior leaflet belly under the enforced pressure and geometric boundary conditions, produced, as closely as possible, the same displacements of the 9 leaflet belly markers as those measured experimentally during time-step Δt_1.

Forward Analysis and Stress-Strain curve—The computed *in vivo* material properties were then used in the finite element model, to determine the stress and strain in the circumferential and radial directions for Δt_1 at marker #14 (as a representative case).

Using marker coordinates at the end of the previous time-step to build the finite element model for the next time-step, a similar inverse finite element analysis was employed to determine the material properties for each time-step during IVR, and forward analysis to determine the stresses and strains were performed for time-steps Δt_2, Δt_3 and Δt_4. The circumferential and radial stresses at marker #14 were plotted against the corresponding circumferential and radial strains at marker #14 for successive time-steps to construct piece-wise circumferential and radial stress-strain curves for each beat.

The linearity of the stress-strain curve for each beat was characterized by the correlation coefficient (r^2) associated with a linear regression analysis of each curve.

Results

Table 1 displays the group mean heart rate, $-dP/dt_{max}$ during IVR, and left ventricular and left atrial pressures for each heart at IVR_1 and IVR_2. Variations in these parameters are seen from heart-to-heart, showing that the stress-strain curves represent a variety of hemodynamic conditions.

Table 2 gives the values of the circumferential and radial stresses and strains for the four transmitral pressure intervals associated with each of the 3 beats for the 8 hearts studied along with the r^2 correlation coefficient values for each curve. Figure 5 displays these data as stress-strain plots, with each panel displaying the circumferential and radial stress-strain relations for each of the three beats from each heart. The group mean (±SD) stress-strain linear correlation coefficient (r^2) values were 0.995±0.003 for the circumferential curves and 0.994±0.003 for the radial curves. The beat-to-beat reproducibility of the stress-strain curves in each heart (Figure 5) validates the robustness of this method to study the stress-strain behavior of the anterior mitral leaflet during IVR. Consistent with results from *ex vivo* testing (May-Newman and Yin, 1995), *in vivo* radial strains are higher than circumferential strains at all time-steps.

Discussion

This study introduces a novel methodology using a combination of inverse and forward finite element analysis for the piece wise construction of stress-strain curves of the mitral valve leaflets, *in vivo*. Sacks and Enomoto (2006) reported, for the first time, the *in vivo* anterior leaflet strains, but the relationship between *in vivo* leaflet stresses and *in vivo* leaflet strains has not been reported thus far. This is the first report of the stress-strain behavior of the anterior mitral valve leaflet in the beating heart. The key finding of the current study is that both circumferential and radial stress-strain curves are linear over a physiologic range of pressures, in the closed mitral valve. This finding validates the material linearity assumption made in our earlier study (Krishnamurthy, Ennis et al., 2008) that determined the *in vivo* material properties of the anterior mitral leaflet during IVR.

The question may arise that because we made use of a linear elastic material model to quantify the material parameters, the overall stress-strain curves during IVR had to be linear. This is not the case. Each time-step analysis was independent. Thus, while each time step yields a modulus based on a linear material model for that time step, the next time-step could yield a completely different modulus. Thus there is no requirement for the combined time-steps to exhibit linear behavior. If the relationship was truly nonlinear, this approach used here should have detected this nonlinearity. Of interest, a prior study (Sacks, Enomoto et al., 2006) also demonstrated linear material behavior of the ovine anterior mitral leaflet in the closed valve, although their results are not directly comparable with the results of the present study as they plotted areal strain against left ventricular pressure,.

Next, we should comment on our choice of a minimum-stress, zero-strain reference state at IVR_2 (Figure 2). First, to the best of our knowledge, it is impossible, using any technique currently available, to measure the loading on each side of the leaflet in the open valve. Moreover, leaflet shape in the open valve varies dramatically as it responds to complex blood flow patterns. Thus, we cannot perform a stress-strain analysis of the leaflet during diastole and thereby cannot establish whether a truly stress-free state exists at any time in an open valve. Thus the current inverse finite element analysis methodology is applicable only to the closed mitral valve, when transleaflet pressures can be defined, and cannot be applied to the open mitral valve when transleaflet pressures are undefined and large geometric non-linearities may be present as observed in *in vitro* studies (He, Sacks et al, 2003;Sacks, He et al, 2002). Second, in order to determine leaflet material properties using inverse FEA, we need to measure transleaflet pressures (both left atrial and left ventricular) over the widest possible range. At IVR_2, left atrial and left ventricular pressures are virtually equal (Figure 2), yet the valve is still closed, thus the conditions at IVR_2 provide the nearest possible approximation to an unloaded state. Further, the interval between IVR_1 and IVR_2 provides the full physiological range of pressures encountered by the closed valve, allowing material properties to be estimated over this wide pressure range. Finally, it is possible, but difficult to imagine, that these thin membranous leaflets, have significant residual stress, relative to the stresses encountered when they are supporting left ventricular pressures, although this possibility remains to be determined. For these reasons, then, we think that the choice of IVR_2 is appropriate as a minimum-stress minimum-strain reference configuration in FEA studies of mitral valve leaflet dynamics.

It must be noted that the leaflet edge has inconsistent deformations and mechanics. Taking this into account, we have reported stresses and strains only for the leaflet belly (*marker 14*, Figure 1), as the belly region of the leaflet is homogeneous and has consistent deformations. In the FEA model, we incorporate the actual motion of the leaflet edge as seen in our experiments in order to enforce accurate boundary conditions to the model, but understanding that the edge behavior is inconsistent we report only the stresses and strains at the center of the leaflet.

Finally, it has to be noted that leaflets are known to be heterogeneous with different regions of the leaflet having different material properties. Strut chordal insertions into the leaflet introduce material heterogeneities in the leaflet (Chen, Yin et al., 2004). Scanning acoustic microscopy indicates that human anterior leaflets are stiffer in the fibrous middle layer than atrial and ventricular layers and the entire leaflet is stiffer at the annulus than at the free edge (Jensen, Baandrup et al., 2006). Leaflet homogeneity was a simplification for this initial effort to quantify the *in vivo* material behavior of the anterior mitral valve leaflet. Developing a heterogeneous finite element model is an ongoing effort in our group.

Acknowledgments

The authors gratefully acknowledge the expert technical assistance of Sigurd Hartnett, BS, Maggie Brophy, AS, Eleazar Briones, BA, Lauren Davis, BS, and George T. Daughters, MS. This study was supported by National Heart, Lung and Blood Institute Grants HL-29589 and HL-67025. Gaurav Krishnamurthy was supported by the BioX Medtronic Graduate Fellowship, Wolfgang Bothe was supported by the Deutsche Herzstiftung, Frankfurt, Germany, and Julia C. Swanson was supported by the Western States Affiliate AHA Postdoctoral Fellowship.

References

Belegundu AD, Damle A, Rajan SD, Dattaguru B, Ville J. Parallel line search in method of feasible directions. Optimization and Engineering 2004;5(3):379–388.

Chen L, McCulloch AD, May-Newman K. Nonhomogeneous deformation in the anterior leaflet of the mitral valve. Ann Biomed Eng 2004;32(12):1599–606. [PubMed: 15675673]

Chen L, Yin FC, May-Newman K. The structure and mechanical properties of the mitral valve leaflet-strut chordae transition zone. J Biomech Eng 2004;126(2):244–51. [PubMed: 15179855]

Daughters GT, Sanders WJ, Miller DC, Schwarzkopf A, Mead CW, Ingels NBJ. A comparison of two analytical systems for 3-D reconstruction from biplane videoradiograms. IEEE Computers in Cardiology 1989;15:79–82.

He Z, Ritchie J, Grashow JS, Sacks MS, Yoganathan AP. In vitro dynamic strain behavior of the mitral valve posterior leaflet. J Biomech Eng 2005;127(3):504–11. [PubMed: 16060357]

He Z, Sacks MS, Baijens L, Wanant S, Shah P, Yoganathan AP. Effects of papillary muscle position on in-vitro dynamic strain on the porcine mitral valve. J Heart Valve Dis 2003;12(4):488–94. [PubMed: 12918852]

Jensen AS, Baandrup U, Hasenkam JM, Kundu T, Jorgensen CS. Distribution of the microelastic properties within the human anterior mitral leaflet. Ultrasound Med Biol 2006;32(12):1943–8. [PubMed: 17169706]

Krishnamurthy G, Ennis DB, Itoh A, Bothe W, Swanson JC, Karlsson M, Kuhl E, Miller DC, Ingels NB Jr. Material properties of the ovine mitral valve anterior leaflet in vivo from inverse finite element analysis. Am J Physiol Heart Circ Physiol 2008;295(3):H1141–H1149. [PubMed: 18621858]

Kunzelman KS, Cochran RP. Stress/strain characteristics of porcine mitral valve tissue: parallel versus perpendicular collagen orientation. J Card Surg 1992;7(1):71–8. [PubMed: 1554980]

Kunzelman KS, Einstein DR, Cochran RP. Fluid-structure interaction models of the mitral valve: function in normal and pathological states. Philos Trans R Soc Lond B Biol Sci 2007;362(1484):1393–406. [PubMed: 17581809]

Levine RA, Handschumacher MD, Sanfilippo AJ, Hagege AA, Harrigan P, Marshall JE, Weyman AE. Three-dimensional echocardiographic reconstruction of the mitral valve, with implications for the diagnosis of mitral valve prolapse. Circulation 1989;80(3):589–98. [PubMed: 2766511]

May-Newman K, Yin FC. Biaxial mechanical behavior of excised porcine mitral valve leaflets. Am J Physiol 1995;269(4 Pt 2):H1319–27. [PubMed: 7485564]

May-Newman K, Yin FC. A constitutive law for mitral valve tissue. J Biomech Eng 1998;120(1):38–47. [PubMed: 9675679]

Niczyporuk MA, Miller DC. Automatic tracking and digitization of multiple radiopaque myocardial markers. Comput Biomed Res 1991;24(2):129–42. [PubMed: 2036779]

Prot V, Skallerud B, Holzapfal G. Transversely isotropic membrane shells with application to mitral valve mechanics. Constitutive modelling and finite element implementation. Int J Numer Methods Eng 2007;71:987–1008.

Sacks MS, Enomoto Y, Graybill JR, Merryman WD, Zeeshan A, Yoganathan AP, Levy RJ, Gorman RC, Gorman JH 3rd. In-vivo dynamic deformation of the mitral valve anterior leaflet. Ann Thorac Surg 2006;82(4):1369–77. [PubMed: 16996935]

Sacks MS, He Z, Baijens L, Wanant S, Shah P, Sugimoto H, Yoganathan AP. Surface strains in the anterior leaflet of the functioning mitral valve. Ann Biomed Eng 2002;30(10):1281–90. [PubMed: 12540204]

Votta E, Caiani E, Veronesi F, Soncini M, Montevecchi FM, Redaelli A. Mitral valve finite-element modelling from ultrasound data: a pilot study for a new approach to understand mitral function and clinical scenarios. Philos Transact A Math Phys Eng Sci 2008;366(1879):3411–34. [PubMed: 18603525]

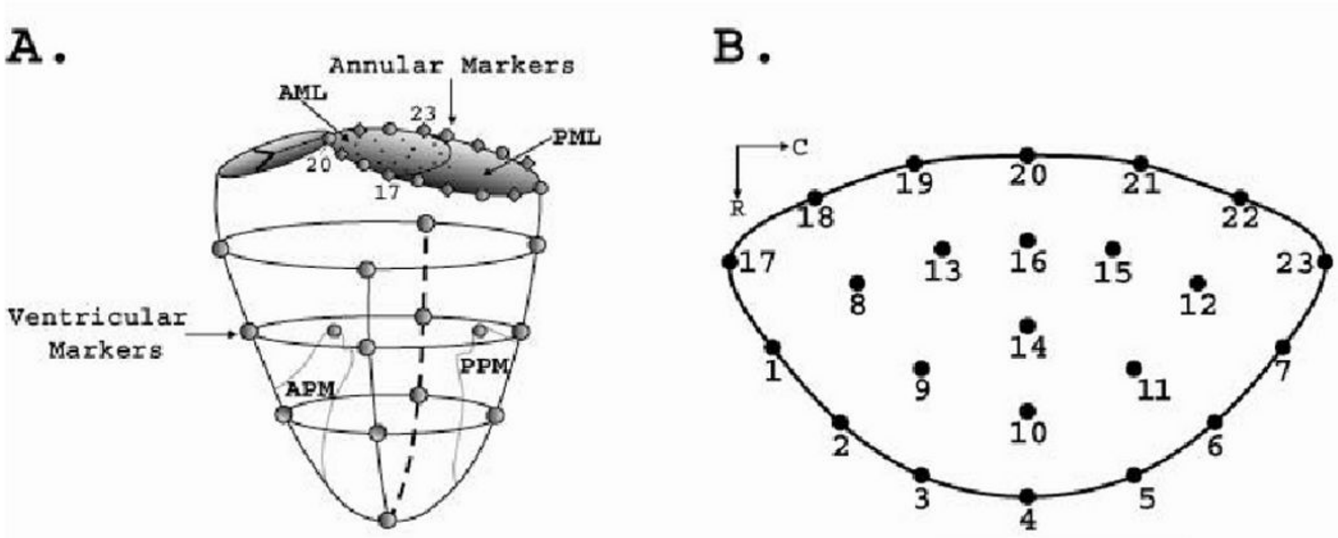

FIGURE 1. Marker Schematic

Figure 1A: Schematic showing ventricular and annular marker locations. Marker 20 is the anterior leaflet saddlehorn marker; markers 17 and 23 are the anterior and posterior commissural marker, respectively. AML= anterior mitral leaflet. PML= posterior mitral leaflet. Figure 1B: Schematic showing anterior leaflet marker grid and circumferential (C) and radial (R) axes.

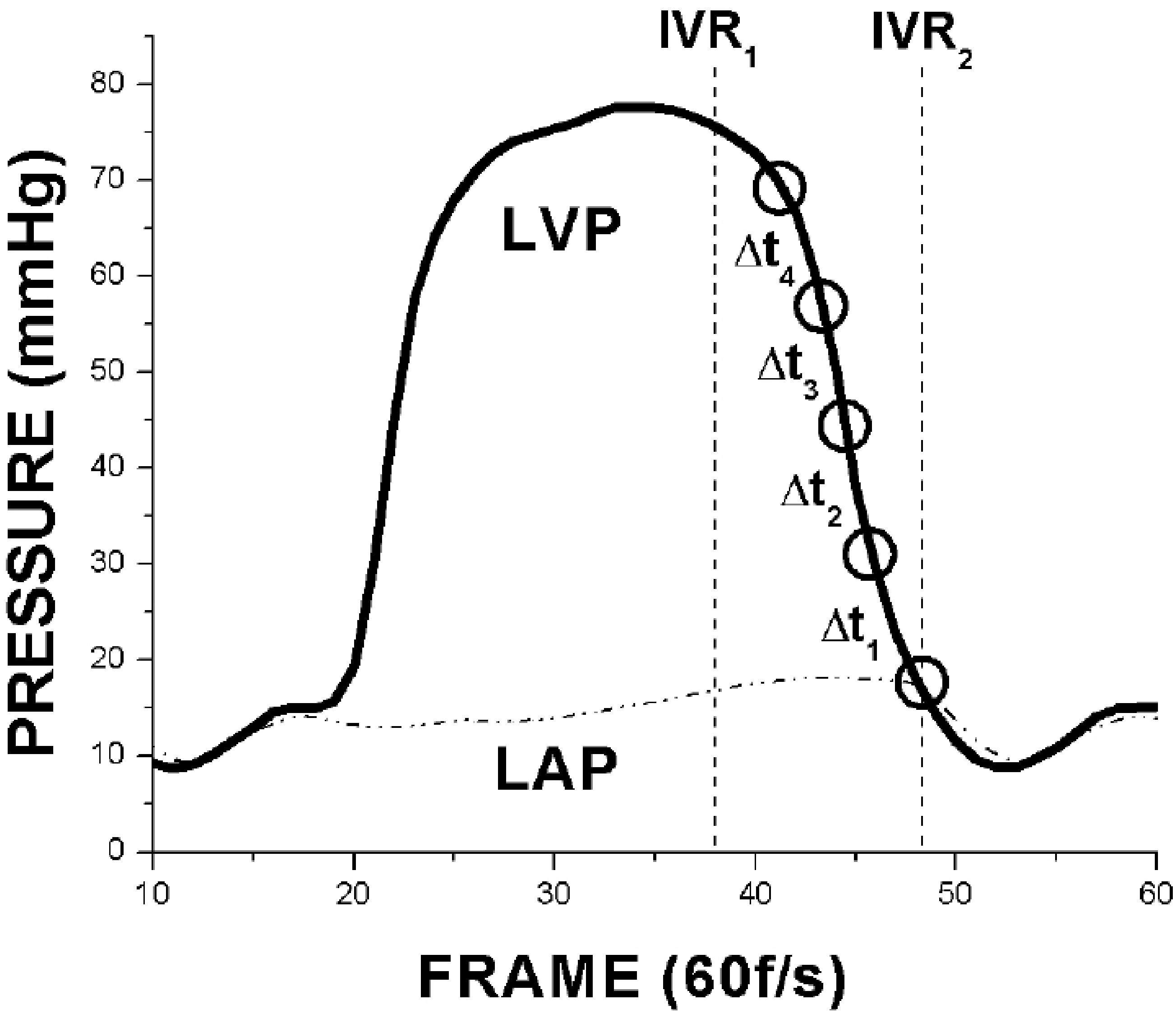

FIGURE 2. Lvp, Lap and Time-Steps

Left ventricular pressure (LVP) and left atrial pressure (LAP) shown for one cardiac cycle. Isovolumic relaxation is defined in the region between IVR_1 and IVR_2. Five frames (open circles) define four time steps (Δt_1-Δt_4) spanning LVP during IVR for each beat.

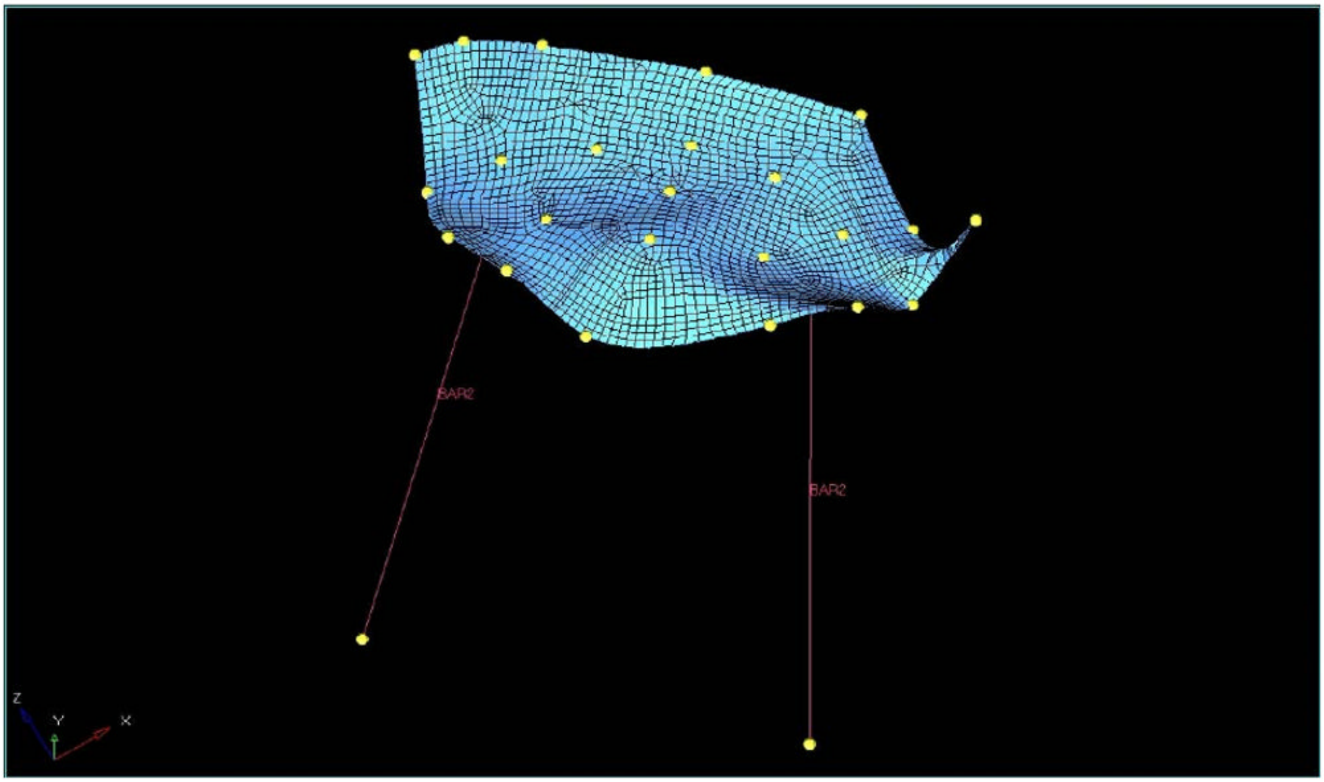

FIGURE 3. Fea Model

Typical finite element model of the anterior mitral valve leaflet. The meshed leaflet surface is depicted in blue. Red lines depict the strut chordae modeled as bar elements. Yellow dots indicate actual marker positions.

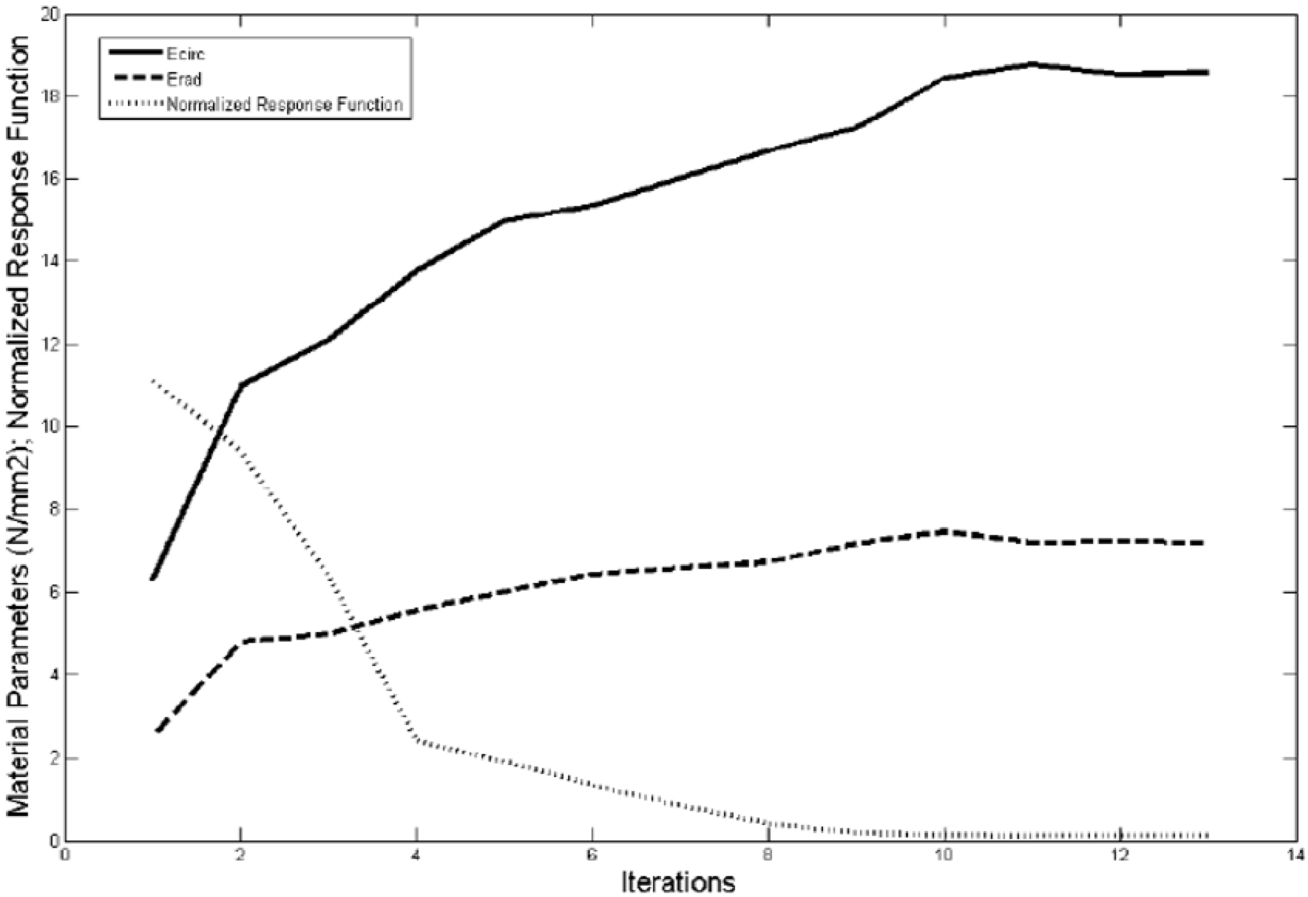

FIGURE 4. Material Parameter Identification

Material properties (E_{circ}, solid line; E_{rad}, dashed line, N/mm^2) and normalized response function (dotted line) versus number of iterations during a typical material parameter identification process.

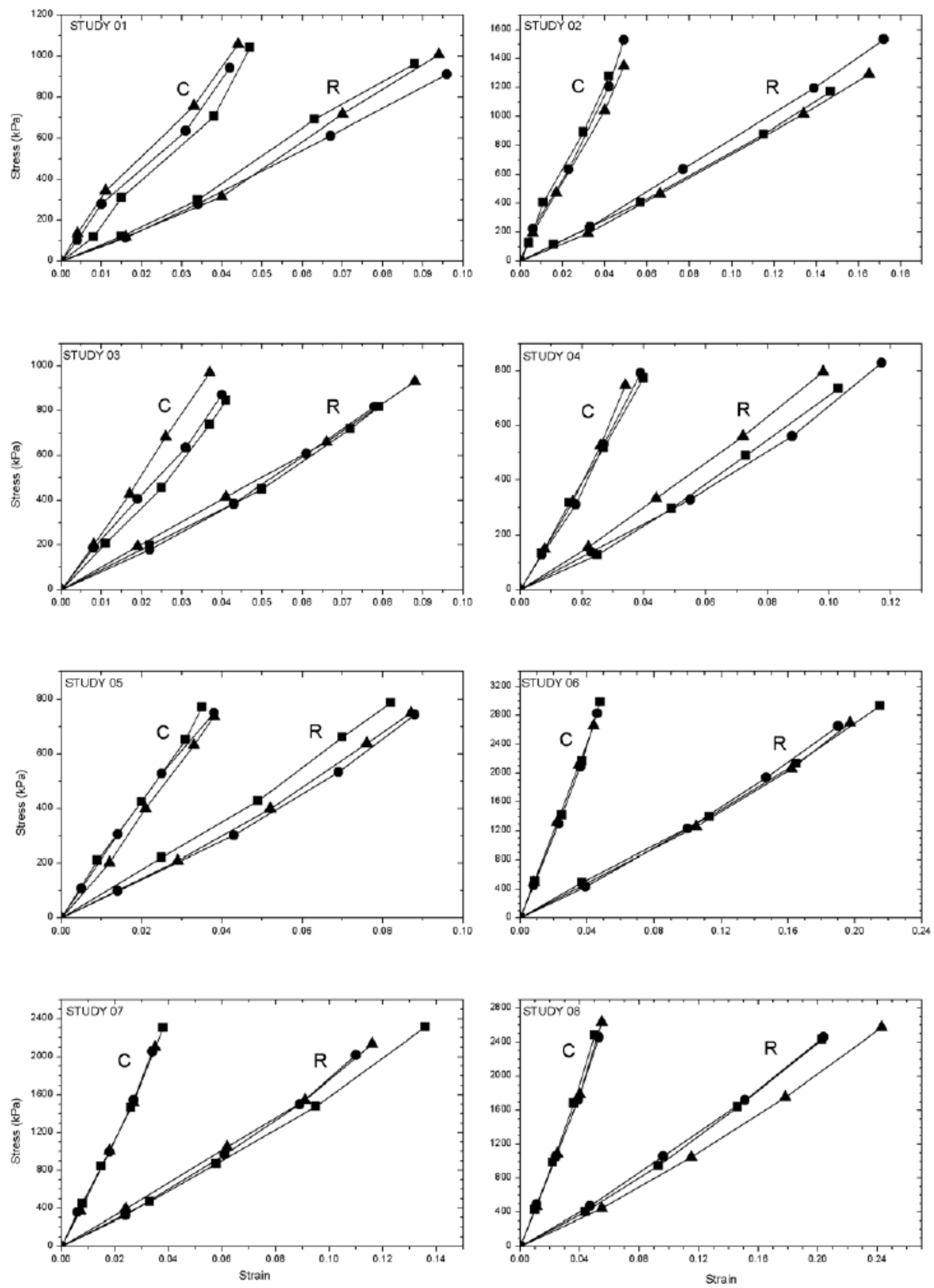

FIGURE 5. Stress- Strain Curves

Stress vs. strain in the radial (R) and circumferential (C) directions. Data in each panel from three beats in specific heart).

NIH-PA Author Manuscript
NIH-PA Author Manuscript

TABLE 1

Hemodynamics

Study	Heart Rate (min^{-1})	$-dLVP/dt_{max}$ (mmHg/s) (IVR)	LVP_{IVR1} (mmHg)	LVP_{IVR2} (mmHg)	LAP_{IVR1} (mmHg)	LAP_{IVR2} (mmHg)
1.	*77*	1592±46	82±1	11±0	10±0	7±1
2.	89	1560±109	92±1	11±1	8±0	8±0
3.	107	1967±123	67±1	10±1	2±0	2±1
4.	93	1103±39	88±1	12±0	14±0	9±0
5.	95	1284±53	87±1	14±1	11±0	12±0
6.	70	991±19	84±1	6±1	8±1	4±1
7.	80	1621±69	84±2	4±1	5±1	4±1
8.	82	1346±327	95±4	7±1	8±0	7±0
Group Mean±S.D	**87±12**	**1433±315**	**85±8**	**9±3**	**8±3**	**7±3**

Heart rate, Negative $dLVP/dt_{max}$ (during IVR) and left ventricular and left atrial pressures at IVR_1 and IVR_2 for the three sequential beats analyzed from each heart.

TABLE 2

Raw Stress and Strain Values

Study	Beat	Time-step	Transmitral Pressure (mmHg)	Circ Stress (kPa)	Circ Strain	r^2 for Circ curves	Radial Stress (kPa)	Radial Strain	r^2 for Radial curves
1.	1	Δt_1	0 → 12	118	0.008		121	0.015	
		Δt_2	12 → 20	310	0.015		300	0.034	
		Δt_3	20 → 49	706	0.038		691	0.063	
		Δt_4	49 → 60	1043	0.047	0.983	963	0.088	0.993
	2	Δt_1	0 → 12	102	0.004		114	0.016	
		Δt_2	12 → 20	279	0.01		279	0.034	
		Δt_3	20 → 49	636	0.031		612	0.067	
		Δt_4	49 → 59	943	0.042	0.991	911	0.096	0.997
	3	Δt_1	0 → 12	136	0.004		118	0.016	
		Δt_2	12 → 20	343	0.011		316	0.040	
		Δt_3	20 → 49	757	0.033		717	0.070	
		Δt_4	49 → 60	1059	0.044	0.992	1006	0.094	0.988
2.	1	Δt_1	0 → 14	124	0.004		117	0.016	
		Δt_2	14 → 32	407	0.011		408	0.057	
		Δt_3	32 → 56	893	0.03		877	0.115	
		Δt_4	56 → 73	1276	0.042	0.996	1172	0.147	0.998
	2	Δt_1	0 → 15	223	0.006		236	0.033	
		Δt_2	15 → 38	635	0.023		637	0.077	
		Δt_3	38 → 67	1207	0.042		1195	0.139	
		Δt_4	67 → 78	1529	0.049	0.997	1534	0.172	0.998
	3	Δt_1	0 → 14	196	0.006		192	0.032	
		Δt_2	14 → 32	473	0.017		468	0.066	
		Δt_3	32 → 56	1039	0.04		1015	0.134	
		Δt_4	56 → 73	1347	0.049	0.993	1292	0.165	0.997
3.	1	Δt_1	0 → 14	208	0.011		198	0.022	
		Δt_2	14 → 37	455	0.025		450	0.050	

Study	Beat	Time-step	Transmitral Pressure (mmHg)	Circ Stress (kPa)	Circ Strain	r^2 for Circ curves	Radial Stress (kPa)	Radial Strain	r^2 for Radial curves
		Δt_3	37 → 54	738	0.037		718	0.072	
		Δt_4	54 → 63	846	0.041	0.995	817	0.079	0.993
	2	Δt_1	0 → 15	187	0.008		179	0.022	
		Δt_2	15 → 28	406	0.019		384	0.043	
		Δt_3	28 → 47	634	0.031		606	0.061	
		Δt_4	47 → 58	871	0.04	0.997	818	0.078	0.991
	3	Δt_1	0 → 14	201	0.008		195	0.019	
		Δt_2	14 → 26	428	0.017		414	0.041	
		Δt_3	26 → 40	682	0.026		660	0.066	
		Δt_4	40 → 56	970	0.037	0.999	931	0.088	0.998
4.	1	Δt_1	0 → 12	132	0.007		128	0.025	
		Δt_2	12 → 26	318	0.016		297	0.049	
		Δt_3	26 → 42	519	0.027		490	0.073	
		Δt_4	42 → 55	774	0.04	0.999	736	0.103	0.992
	2	Δt_1	0 → 11	127	0.007		138	0.023	
		Δt_2	11 → 23	312	0.018		330	0.055	
		Δt_3	23 → 39	531	0.027		561	0.088	
		Δt_4	39 → 57	792	0.039	0.995	830	0.117	0.991
	3	Δt_1	0 → 12	149	0.008		156	0.022	
		Δt_2	12 → 27	320	0.017		334	0.044	
		Δt_3	27 → 43	526	0.026		560	0.072	
		Δt_4	43 → 56	748	0.034	0.992	797	0.098	0.998
5.	1	Δt_1	0 → 14	211	0.009		221	0.025	
		Δt_2	14 → 33	424	0.02		428	0.049	
		Δt_3	33 → 46	653	0.031		661	0.07	
		Δt_4	46 → 57	772	0.035	0.997	788	0.082	0.996
	2	Δt_1	0 → 12	108	0.005		99	0.014	
		Δt_2	12 → 29	305	0.014		302	0.043	

NIH-PA Author Manuscript
NIH-PA Author Manuscript

Study	Beat	Time-step	Transmitral Pressure (mmHg)	Circ Stress (kPa)	Circ Strain	r^2 for Circ curves	Radial Stress (kPa)	Radial Strain	r^2 for Radial curves
		Δt_3	29 → 44	528	0.025		533	0.069	
		Δt_4	44 → 59	750	0.038	0.997	744	0.088	0.991
	3	Δt_1	0 → 14	201	0.012		209	0.029	
		Δt_2	14 → 33	399	0.021		398	0.052	
		Δt_3	33 → 46	632	0.033		639	0.076	
		Δt_4	46 → 57	738	0.038	0.998	750	0.087	0.994
6.	1	Δt_1	0 → 17	448	0.008		468	0.033	
		Δt_2	17 → 31	843	0.015		871	0.058	
		Δt_3	31 → 49	1466	0.026		1478	0.095	
		Δt_4	49 → 68	2302	0.038	0.997	2311	0.136	0.994
	2	Δt_1	0 → 15	357	0.006		329	0.024	
		Δt_2	15 → 37	996	0.018		967	0.061	
		Δt_3	37 → 56	1544	0.027		1500	0.089	
		Δt_4	56 → 71	2056	0.034	0.997	2019	0.11	0.992
	3	Δt_1	0 → 15	372	0.007		392	0.024	
		Δt_2	15 → 36	1008	0.018		1044	0.062	
		Δt_3	36 → 54	1515	0.027		1543	0.091	
		Δt_4	54 → 69	2098	0.035	0.997	2135	0.116	0.995
7.	1	Δt_1	0 → 14	427	0.01		403	0.044	
		Δt_2	14 → 30	986	0.022		944	0.093	
		Δt_3	30 → 45	1689	0.036		1643	0.146	
		Δt_4	45 → 58	2485	0.05	0.997	2430	0.203	0.993
	2	Δt_1	0 → 15	492	0.011		472	0.047	
		Δt_2	15 → 32	1057	0.024		1061	0.096	
		Δt_3	32 → 47	1728	0.039		1722	0.151	
		Δt_4	47 → 61	2457	0.053	0.998	2461	0.204	0.997
	3	Δt_1	0 → 15	468	0.011		445	0.055	
		Δt_2	15 → 33	1090	0.025		1050	0.115	

Study	Beat	Time-step	Transmitral Pressure (mmHg)	Circ Stress (kPa)	Circ Strain	r^2 for Circ curves	Radial Stress (kPa)	Radial Strain	r^2 for Radial curves
		Δt_3	33 → 48	1789	0.04		1753	0.178	
		Δt_4	48 → 62	2636	0.055	0.996	2574	0.243	0.993
8.	1	Δt_1	0 → 13	512	0.009		488	0.037	
		Δt_2	13 → 32	1415	0.025		1400	0.113	
		Δt_3	32 → 49	2163	0.037		2133	0.165	
		Δt_4	49 → 64	2985	0.048	0.996	2934	0.215	0.996
	2	Δt_1	0 → 13	454	0.008		433	0.039	
		Δt_2	13 → 33	1299	0.023		1234	0.1	
		Δt_3	33 → 51	2091	0.036		1942	0.147	
		Δt_4	51 → 67	2827	0.046	0.997	2651	0.19	
	3	Δt_1	0 → 14	488	0.008		455	0.038	
		Δt_2	14 → 33	1321	0.022		1261	0.105	
		Δt_3	33 → 51	2110	0.035		2062	0.162	
		Δt_4	51 → 66	2659	0.044	0.999	2696	0.197	0.994

Stress and strain values for each time-step for 3 beats, 8 hearts, and 4 time intervals (Δt1- Δt4) The transmitral pressure gradient, circumferential (Circ) stress and strain, radial stress and strain and r^2 values for each stress-strain curve are shown.